2.L

Nuclear Physics **79** (1966) 609—624; © *North-Holland Publishing Co., Amsterdam*

PROTON-NUCLEI CROSS SECTIONS AT 20 GeV

G. BELLETTINI, G. COCCONI, A. N. DIDDENS, E. LILLETHUN †,
G. MATTHIAE ††, J. P. SCANLON ††† and A. M. WETHERELL
CERN, Geneva

Received 30 September 1965

Abstract: Measurements of the differential cross section of 20 GeV protons scattered elastically and quasi-elastically by a series of nuclei, ranging from Li to U, are presented. The total and the elastic cross sections are also given.

The light nuclei show, at the smallest angles, the characteristic central diffraction peak produced by an absorbing disc; at larger angles the quasi-elastic scattering produced by single nucleons predominates. The heavy nuclei exhibit diffraction rings up to the largest angles explored (≈ 20 mrad).

The diffraction patterns are interpreted with an optical model that takes into account the contribution of both the nuclear and the Coulomb interactions. The radii of the heaviest nuclei turn out to be consistently larger than those deduced from electron scattering experiments. The opacity is found to be nearly complete only in the heaviest nuclei.

Results at the largest angles measured show that only a small fraction of the nucleons in the nuclei can act as effectively independent scattering centres.

E | NUCLEAR REACTIONS ^{6}Li, ^{7}Li, ^{9}Be, Al, Cu, Pb, U(p, p), $E = 19.2$ GeV, ^{12}C(p, p), $E = 21.5$ GeV; measured $\sigma(\theta)$, $\sigma_{\mathrm{p,t}}$, Deduced $\sigma_{\mathrm{p,el}}$, $\sigma_{\mathrm{p,abs}}$, nuclear radii.

1. Introduction

The elastic scattering of protons by nuclei has been studied since the operation of the earliest accelerators. At energies above some hundreds of MeV, i.e., above the threshold for meson production, it has been found that the most convenient interpretations of the data are based on optical models as at these energies diffraction phenomena become predominant as a consequence of the strong absorption of the protons by nuclear matter. On general grounds, optical models should be better the higher the energy of the protons, as the approximations introduced in the calculations are better fulfilled the smaller the wave length. At 3 GeV, the highest energy at which systematic experiments were so far performed [1]), an optical model was applied quite satisfactorily ‡.

The results of the experiments presented here for 19.3 GeV/c protons on ^{6}Li, ^{7}Li, ^{9}Be, ^{27}Al, $^{63.6}$Cu, $^{207.2}$Pb and $^{238.0}$U and for 21.5 GeV/c protons on ^{12}C

† Present address: University of Bergen, Bergen, Norway.
†† On leave of absence from Istituto Superiore di Sanità, Rome, Italy.
††† Present address: AERE Harwell, Didcot, Berks., England.
‡ In ref. [1]), the earlier literature is also quoted.

emphasize the importance of diffraction phenomena. At such energies, provided the angular resolution is sufficiently good, the scattering produced coherently by the whole nucleus and the incoherent scattering of the protons on the individual nucleons of the nuclei, the so-called quasi-elastic scattering, can be neatly separated. The coherent scattering predominates at the smallest angles, the incoherent scattering at the largest.

In sect. 2, the kinematics and the sensitivity of the experiment to elastic, quasi-elastic and inelastic scattering processes are discussed. The experimental apparatus is described in sect. 3, and the results obtained with light and with heavy nuclei are presented in sect. 4 and 5, respectively. Finally, the values for the total and the elastic cross sections which can be deduced from the measurements are discussed in sect. 6.

2. Discussion of the Method

Let p_0 be the momentum of the incoming proton in the lab system and p the momentum of the outgoing proton scattered elastically at an angle Θ by a particle of mass M. At highly relativistic energies and at angles $\Theta \ll 1$, the squared four-momentum transfer t is given to a very good approximation by the expression

$$|t| \approx p_\perp^2 = p^2\Theta^2 \approx p_0^2\Theta^2, \tag{1}$$

where $p_\perp$ is the transverse momentum of the scattered proton.

The kinetic energy of the recoiling particle is

$$T = \frac{|t|}{2M}, \tag{2}$$

and the momentum lost by the proton, in the same approximation, is

$$\Delta p = p_0 - p = \frac{p_\perp^2}{2Mc} = \frac{T}{c}. \tag{3}$$

When the target is excited to a level of energy $\Delta E \ll mc^2$ (m is the proton mass), the proton four-momentum transfer is still given at highly relativistic energies by eq. (1). The momentum loss becomes however

$$\Delta p \approx \frac{|t|}{2Mc} + \frac{\Delta E}{c}. \tag{4}$$

In the present experiment the momenta p and p_0 were measured with an accuracy of ± 50 MeV/c; the recoiling particle was not detected at all. Thus, while scattering events in which mesons were produced were excluded, as in that case Δp would have differed by more than 140 MeV/c from the values expected for elastic events, the events where the target nucleus was left in an excited state were not resolved from the true elastic events, nor from those in which a single nucleon was knocked off the nucleus. For example, when a 20 GeV/c proton is scattered at an angle of 15 mrad by a medium size nucleus, its momentum changes by 1 MeV/c if the nucleus recoils and by 50 MeV/c if only one nucleon recoils; still the resolution of the present experiment was not sufficient to distinguish the two cases.

On the other hand, it is expected that the scattering events with $\Theta < 7$ mrad ($|t| < 0.02$ (GeV/c)^2) are predominantly those in which the nucleus remains close to its fundamental state (coherent-elastic scattering) because in this case the single nucleons cannot recoil with enough energy to leave the nucleus. The events at larger angles, instead, can also be due to cases in which one of the nucleons present in the nucleus recoils violently enough to break the nuclear bond of ≈ 8 MeV (incoherent elastic or quasi-elastic scattering). Thus the results of this experiment at the smallest angles give information about nuclear form factors, while those at the largest angles can give information about the probability that proton-nucleon elastic collisions take place in the nucleus.

3. The Experimental Technique

The experimental apparatus is shown in fig. 1 and is the same as that used for the measurement of proton-proton small-angle scattering [2]). A system of quadrupoles and bending magnets (not shown in the figure) transported a well collimated and rather monochromatic beam of protons (average momentum 19.3 GeV/c) from the

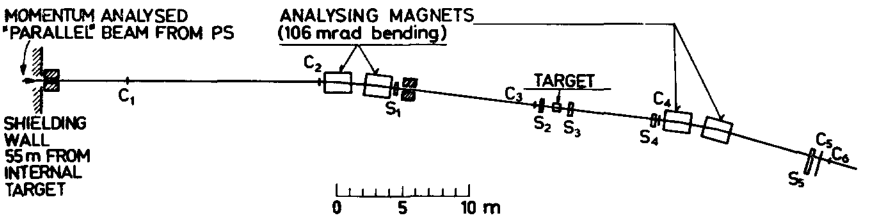

Fig. 1. Experimental layout.

CERN proton synchrotron to the experimental area. The incident proton beam, 5 mm in diam and generally containing about 1000 particles per pulse (the duration of each pulse was 0.2 sec and the repetition rate was $\frac{1}{2}$ sec^{-1}), was defined by scintillation counters C_1, C_2 and C_3 and the scattered protons were detected by counters C_4 and C_5. The scintillator C_4, which defined the solid angle accepted by the system, had a hole allowing unscattered particles to pass through without detection. The minimum scattering angle defined by this counter was usually 1.5 mrad; however, for the study of Cu and Pb scattering at angles above 5 mrad, it was increased to 4 mrad. The maximum scattering angle accepted was ≈ 20 mrad. The background trigger rate from unscattered particles was reduced by a small anticoincidence counter C_6 directly in the path of the beam. The coincidence signature used to trigger the spark chambers in the scattering runs was $1\,2\,3\,4\,5\,\bar{6}$.

Multiple scattering and background throughout the system were reduced to a very low level by transporting the beam in vacuum and by minimizing the thickness of scintillators, vacuum windows and spark chamber plates.

The positions of the incident and scattered protons were measured to about ± 0.3 mm by sonic spark chambers [3]), S_1 to S_5. Each spark chamber had two gaps, four piezo-electric transducers detecting the sound signals in each gap. The forty sonic times-of-flight, digitized in units of 0.5 μs, were first registered in a magnetic core memory and subsequently transferred to a SDS 920 computer connected on-line [3,4]), together with other data such as the number of beam particles leading up to a spark chamber trigger. Up to 12 events per synchrotron pulse could be collected; between pulses the computer performed simple tests to check the operation of the electronics and of the spark chambers. The accepted data were recorded on magnetic tape for the subsequent complete analysis with the CERN IBM 7090 computer.

Calibration runs, using the coincidence trigger 1 2 3 5 and no target, giving the mean positions of the unscattered beam in the spark chambers, were made at regular intervals and the scattering angles and momenta were obtained with reference to these mean positions.

As a result of the care taken in reducing multiple scattering and of the good spatial resolution in the spark chambers, the angular resolution function of the system for unscattered protons was found to fall to 10% at 0.15 mrad and the full width at half height of the distribution of the momentum difference between incoming and outgoing protons was about 0.4%.

Absolute differential elastic scattering cross sections were obtained from the number of particles included within the elastic peaks in the momentum distribution of the scattered protons and the total number of beam particles. Uncertainties created by the inclusion within our limits of events with meson production were always less than 1%.

The high precision in angle determination made it possible to compute the point of interaction for scattering events to about ± 10 cm in longitudinal position. The events associated with scattering in the scintillator and spark chamber material at each end of the target were removed by rejecting events having interaction points clearly outside the space occupied by the target. Background measurements using no target were also performed. The residual background to be subtracted, e.g. for the C target, was about 0.3% for elastic events between 2 and 3 mrad and remained small at larger angles.

4. Results of Measurements with Light and Medium Nuclei

In this section the results with ^{6}Li, ^{7}Li, ^{9}Be, ^{12}C and ^{27}Al are discussed. The measurements on C were done with 21.5 GeV/c protons; the others with 19.3 GeV/c protons. The thickness of the targets (e.g. 4 g $\cdot$ cm^{-2} for Li) were such that, within the smallest angular interval (2 to 3 mrad), the contribution of the plural Coulomb scattering was less than 10% of that due to single scattering. At larger angles the relative importance of plural scattering decreased rapidly and became smaller than 1% at $\Theta > 5$ mrad. Multiple and plural scatterings were evaluated with the Molière theory, using the formulae given by Bethe and Ashkin [5]). The data presented below

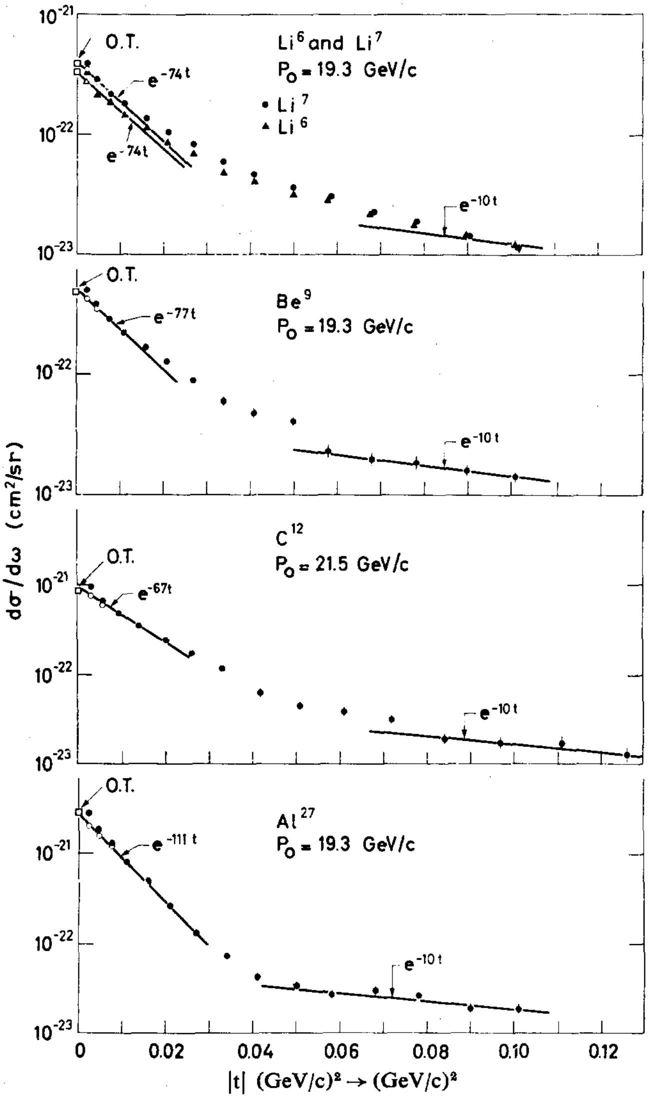

Fig. 2. Differential cross sections plotted as a function of the four-momentum transfer squared. Black dots: experimental results; open circles: experimental cross sections after subtraction of the Coulomb contribution; O.T.: optical theorem cross section evaluated using total cross sections of table 1. For each element the steep line fitting the first points gives the nuclear form factor. The lines through the points with the largest values of $|t|$ all have the slope, (10 (GeV/c)^2), exhibited by the proton-proton differential cross section.

are corrected for plural and multiple scatterings, as well as for other small effects, like self-absorption of the protons in the target and no target background, but not for single Coulomb scattering. For each nucleus from 10 000 to 40 000 elastic scattering events were measured.

In fig. 2 the differential cross sections are plotted as functions of the four-momentum transfer squared. The errors quoted are only statistical. The most striking feature for all elements is the sudden decrease of the cross section as $|t|$ varies from zero to ≈ 0.03 $(\mathrm{GeV}/c)^2$. This is due to the strong angular dependence of both the Coulomb and the diffraction differential cross sections for coherent nuclear scattering. A more gentle decrease follows this rapid variation and is to be attributed to the incoherent scattering of the protons from the single nucleons of the nuclei.

A rather simplified and approximate analysis of the data will now be given, which has the advantage of allowing an immediate physical interpretation and of being sufficiently accurate for analysing the results on light and medium nuclei. In sect. 5 a more elaborate optical model will be used for the heavy nuclei.

Within the region of $|t| < 0.03$ $(\mathrm{GeV}/c)^2$, the contributions of the Coulomb and of the coherent diffraction scattering are given by the equations:

$$\frac{\mathrm{d}\sigma}{\mathrm{d}\omega} = C^2 + I^2 + R^2 + 2CR, \tag{5}$$

where

$$C^2 = Z^2 \frac{(2r_e pmc)^2}{t^2} F_{\mathrm{C}}^2(A, t)$$

is the Rutherford formula multiplied by the square of the Coulomb form factor $F_{\mathrm{C}}(A, t)$. It represents the contribution of the Coulomb scattering of the protons by a nucleus of charge Z and atomic number A, and in this approximation it is considered completely real. The quantity

$$I^2 = \left(\frac{p\sigma_{\mathrm{tot}}}{4\pi\hbar}\right)^2 F_{\mathrm{n}}^2(A, t)$$

is the square of the imaginary part of the coherent nuclear scattering amplitude. Here $F_{\mathrm{n}}^2(A, t)$ is the strong interaction nuclear form factor, which is to be deduced, and σ_{tot} the total cross section due to nuclear interaction, excluding the Coulomb contribution. It is assumed that this separation can be carried out. Finally, R is the real part of the coherent nuclear scattering amplitude that may be expected to be different from zero, since at these energies the proton-proton elastic scattering indicates the existence of a sizeable real amplitude [2]. However, utilizing the values of the total nuclear cross sections σ_{tot} measured in this experiment (see sect. 6) for deriving the value of I at the forward direction, it was found that the experimental differential cross sections on light and medium nuclei can be interpreted assuming that the quantity R is small in comparison to I and C; consequently, the data will be analysed with the assumption that $R = 0$, thus dropping the last two terms of eq. (5). With the reduced form of eq. (5)

$$\frac{\mathrm{d}\sigma}{\mathrm{d}\omega} = Z^2 \left(\frac{2r_e pmc}{t}\right)^2 F_{\mathrm{C}}^2(A, t) + \left(\frac{p\sigma_{\mathrm{tot}}}{4\pi\hbar}\right)^2 F_{\mathrm{n}}^2(A, t), \tag{6}$$

the Coulomb and the nuclear contributions can be separated.

For the elements under discussion, a Gaussian form factor

$$F_{\mathrm{C}}^2(A, t) = \exp\left(-\frac{a^2}{3\hbar^2}|t|\right) \tag{7}$$

was used for the Coulomb form factor, and the values for a were taken from the work of Herman and Hofstadter [6]). The main criticism that can be made of this choice is that the Herman and Hofstadter form factors are valid for electron-nuclear scattering, i.e. for particles that can penetrate undisturbed into nuclear matter, while high-energy protons cannot. This effect will make the proton-nucleus form factor smaller, and the more so the larger is t, and for equal t, the heavier is the element. However, as will be discussed in the following section, the approximation adopted here is acceptable for light and medium nuclei and for the angular ranges explored in the present experiment.

In fig. 2 the open circles were obtained by subtracting from the experimental points (the black dots) the contribution of the Coulomb scattering evaluated according to eqs. (6) and (7). After this correction is applied, the experimental points at the smallest t values are well fitted (see fig. 2) by a straight line, and in all cases these lines intersect the $t = 0$ ordinate at a point which is compatible with the optical theorem value

$$\left(\frac{\mathrm{d}\sigma}{\mathrm{d}\omega}\right)_{t=0} = \left(\frac{p\sigma_{\mathrm{tot}}}{4\pi\hbar}\right)^2. \tag{8}$$

This means, as was mentioned earlier, that there is no indication of a sizeable real part in the amplitude of the coherent nuclear diffraction scattering. In addition these straight lines show that, at least for $|t| < 0.03\ \mathrm{GeV}/c)^2$, the nuclear form factor is given by the expression

$$F_{\mathrm{n}}^2(A, t) = \mathrm{e}^{-B|t|}. \tag{9}$$

Eq. (9) with $B = R^2/4\hbar^2$ is the small argument expansion of the form factor expected for the diffraction by a spherical black body of radius R, which is the familiar optical model expression

$$F_{\text{black body}}^2 = \left(\frac{2J_1(kR\Theta)}{kR\Theta}\right)^2 = \left(\frac{2J_1\left(\frac{R}{\hbar}\sqrt{|t|}\right)}{\frac{R}{\hbar}\sqrt{|t|}}\right)^2. \tag{10}$$

The correctness of this interpretation is confirmed both by the reasonable values of the nuclear radii obtained and by the fact that, when other diffraction maxima besides that at $\Theta = 0$ begin to appear in the curves of fig. 2, these maxima occur at the positions predicted by eq. (10), that is for

$$\frac{R}{\hbar}\sqrt{|t|} = kR\Theta = 0; 5.14; 8.42; 11.62, \text{etc.}, \tag{11}$$

where

$$k = p/\hbar = 5.06\ p\ (\text{fm})^{-1}, \qquad (p \text{ in GeV}/c).$$

TABLE 1

Cross sections

	R (fm)	σ_{tot} (b)	σ_{el} [a] (b)	σ_{abs} (b)	$N(A)$	$N(A)/A$	$1-\frac{\sigma_{abs}}{\pi R^2}$
^{6}Li	3.40 ± 0.10	0.232 ± 0.005	0.038	0.194	3.0	0.50	0.47
^{7}Li	3.40 ± 0.10	0.250 ± 0.005	0.042	0.208	3.0	0.43	0.43
^{9}Be	3.47 ± 0.15	0.278 ± 0.004	0.051	0.227	3.5	0.39	0.41
^{12}C	3.24 ± 0.10	0.335 ± 0.005	0.081	0.254	3.4	0.28	0.25
^{27}Al	4.15 ± 0.10	0.687 ± 0.010	0.215	0.472	4.6	0.17	0.15
$^{63.6}$Cu	5.60 ± 0.10	$1.36\ \pm 0.02$	0.51	0.85	6.7	0.10	0.16
$^{207.2}$Pb	7.50 ± 0.25	$3.29\ \pm 0.10$	1.54	1.75	(9.5)	(0.046)	0.00
$^{238.0}$U	7.50 ± 0.40				(10)		

[a]) Nuclear coherent only. The errors on σ_{el} are about $\pm 5\,\%$.

The nuclear radii that can be deduced by means of a least-squares fit to the slopes of the primary maxima are listed in table 1, column 1. A comparison with the values given by Herman and Hofstadter [6]) for the "equivalent uniform model" shows good agreement for light elements.

The steep decrease at small angles produced by the nuclear diffraction scattering is followed at large angles by a continuous and much less steep decrease of the differential cross sections. This behaviour indicates that the incoherent elastic scattering from the individual nucleons in the nuclei (quasi-elastic scattering) replaces the coherent nuclear scattering at large angles; indeed the large angle slope is about that characteristic of free nucleon-nucleon scattering.

Fig. 2 shows that the contribution of quasi-elastic scattering increases very little when going from the lighter to the heavier elements. This is the fact that makes it possible to observe the appearance of the secondary diffraction rings in the heavier elements. The reason is that a secondary ring becomes visible only when, with increasing mass number, the coherent cross section rises enough to bring the secondary maxima above the nearly constant level of the incoherent background.

For the scattering at the largest angles, which is attributed to the incoherent proton-nucleon scattering, the following procedure was applied. On the basis of what is known about proton-proton scattering [2]) and assuming that proton-proton and proton-neutron scatterings are the same and neglecting the real part of the scattering amplitude, it can be expected that the incoherent scattering cross section has the form

$$\left(\frac{d\sigma}{d\omega}\right) = N(A)\left(\frac{p\sigma_{\mathrm{tot}}(\mathrm{pp})}{4\pi\hbar}\right)^2 \exp\left(-C|t|\right), \tag{12}$$

where C is a constant independent of A. Here the term $p\sigma_{\mathrm{tot}}(\mathrm{pp})/4\pi\hbar$ expresses the proton-proton forward scattering amplitude, the exponential describes the behaviour of the proton-proton differential cross section, and $N(A)$ is the number of free nucleons that at large angles produce the same scattering produced incoherently by the nucleus of mass number A. In other words, the scattering observed outside the coherence region is made equal to the scattering produced by $N(A)$ nucleons, each one operating independently. Using for the forward scattering amplitude and for C the numerical values [2]) found for the proton-proton scattering at $p_0 = 19.3$ GeV/c, and expressing t in (GeV/c)^2, eq. (12) reads

$$\frac{d\sigma}{d\omega} = N(A)\, 11.0\, \mathrm{e}^{-10|t|}\ \mathrm{b/sr}. \tag{13}$$

In fig. 2, straight lines having the slope given by (13) were fitted to the cross sections measured at the largest $|t|$, and from those fits the values of $N(A)$ of column 5 of table 1 were deduced.

A satisfactory description of the dependence of $N(A)$ on A is given by the expression

$$N(A) = 1.6\, A^{\frac{1}{3}}. \tag{14}$$

This relation shows that the number of equivalent free nucleons increases, at least in first approximation, as the circumference of the nucleus. This result has a simple geometrical interpretation; namely that the proton can emerge with full energy only when it hits a nucleon situated on the rim of the nucleus.

It is also possible to look at the incoherent diffraction scattering from a different point of view. Since all nucleons present in a target of atomic number A are condensed in nuclei, and since in large momentum transfer elastic scattering events each nucleon can be considered as free from nuclear bonds, the quantity $N(A)/A$ represents the fraction of cases in which the proton of momentum p_0 crosses the nucleus without being absorbed by inelastic interactions. Thus $N(A)/A$ is the quantity which in an optical model is called the transparency of the nucleus, i.e. the quantity $1-(\sigma_{\mathrm{abs}}/\pi R^2)$.

In columns 6 and 7 of table 1 the values of these two quantities are given and are evaluated using the numbers of the other columns of the same table. The good consistency between the two sets of values gives credit to this interpretation. Actually, in our opinion the transparency given by $N(A)/A$ is a better determined quantity than that defined otherwise.

The comparison between the cross sections measured for ^{6}Li and ^{7}Li is also interesting. The extra neutron present in ^{7}Li affects the coherent elastic scattering but, consistent with eq. (14), does not appreciably affect the incoherent scattering.

5. Heavy Nuclei

The results obtained for targets of $^{63.6}$Cu, $^{207.2}$Pb and $^{238.0}$U are given in fig. 3, after correction for multiple scattering and self-absorption. The secondary diffraction

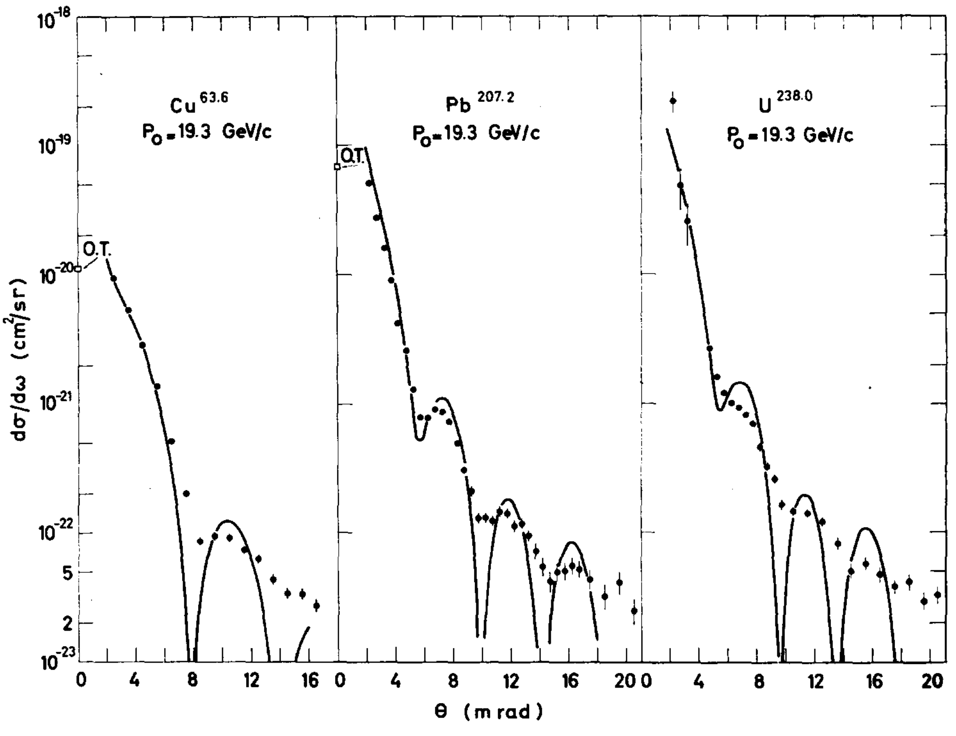

Fig. 3. Diffraction cross sections for the heavy nuclei plotted as a function of angle. The optical theorem points (O.T.) are deduced from the total cross sections of table 1. The curves are calculated using eqs. (15)–(19) and the numerical values presented in table 1.

rings are clearly visible. From the values of Θ at which the maxima occur and from relations (11) the nuclear radii given in table 1 for Pb and U were obtained.

In order to explain the magnitude of the cross sections observed it is necessary to take into account the absorption of the protons in the nucleus, in the evaluation of the Coulomb and of the nuclear form factors.

In describing the calculations that have been performed, we follow the presentation of Clementel and Coen [7]) and use their notations. The general expression for the elastic scattering differential cross section of a charged particle of momentum $p = \hbar k$ is

$$\frac{d\sigma}{d\omega} = |f(\Theta)|^2 = \left| \frac{1}{2ik} \sum_{l=0}^{\infty} (2l+1)\{\exp[2i(\eta_l+\delta_l)]-1\}P_l(\cos\Theta) \right|^2, \tag{15}$$

where η_l are the phase shifts due to the Coulomb field and δ_l those due to the nuclear field.

If it is assumed that the nuclear matter is distributed within a sphere of radius $R = l_C/k$, the terms present in eq. (15) can be divided in two groups, one containing the term with $l > l_C$ and the other those with $l < l_C$. The contribution coming from the terms with $l > l_C$ was calculated by Clementel and Coen by putting

$$\eta_l = n \log l, \qquad \delta_l = 0 \qquad \left(n = \frac{Ze^2}{\hbar\beta c}\right) \tag{16}$$

and is given by the expression

$$(\Theta) = -\frac{1}{k\Theta^2}\left\{2n \exp[i(2\eta_0 - 2n \lg \tfrac{1}{2}\Theta)] + l_c\Theta \exp[i(2n \lg l_c - \tfrac{1}{2}\pi)]J_1(l_c\Theta) - 2n \exp[-i2n \lg \Theta] \int_0^{l_c\Theta} y^{2in} J_1(y)dy\right\}, \tag{17}$$

where $\eta_0 = -nC$ and $C = 0.5772$ is Euler's constant. For 19.3 GeV/c protons on, e.g. Pb, $l_C = 670$.

In order to evaluate the waves with $l < l_C$, eq. (15) was used, taking into account also the nuclear transparency. The nuclear charge distribution, following Bethe [8]), was assumed to be Gaussian. The Coulomb phase shifts are then given by the expression

$$\eta_l = n\left[\log l + \int_{l/ka}^{\infty} \frac{dx}{(x^2 - l^2/k^2a^2)^{\frac{1}{2}}}\{1-\operatorname{erf}(x)\}\right], \tag{18}$$

where $\sqrt{\frac{3}{2}}\,a$ is the r.m.s. radius of the nuclear charge distribution as given by Herman and Hofstadter [6]). The nuclear phase shifts inside the nucleus were taken as complex

$$\delta_l = \alpha_l + i\beta_l.$$

If there is a real scattering amplitude, $\alpha_l \neq 0$. The imaginary part β_l is related to the transparency of the nuclear matter for the incoming proton. We have used the classical relation (straight line approximention in uniform nuclear matter)

$$2\beta_l = \frac{\sqrt{l_C^2 - l^2}}{k\lambda}. \tag{19}$$

The mean free path, λ, of the incoming protons in nuclear matter was chosen by requiring that, at the end of the computation, the absorption cross section of the nucleus be equal to that measured and listed in table 1. The numerical calculations were carried out using the CERN IBM 7090 computer.

In heavy nuclei it is difficult to extract information on the real part of the scattering amplitude by extrapolating the differential cross section to zero angle because the steep dependence of the nuclear form factor on the angle makes the interpretation of the data strongly model-dependent. For Cu, however, the analysis is still valid. The cross sections measured from 2.5 to 5.5 mrad, after correction for the Coulomb contribution, were evaluated by means of eqs. (15)–(19) assuming zero real scattering amplitude. When fitted with a Gaussian form factor (eq. (9)), these corrected cross sections gave for Cu the radius quoted in table 1, and an intersection with the $t = 0$ axis coinciding, within the errors, with the optical theorem point. The value of R found for Cu in this way is in agreement with that deduced from the location of the first diffraction ring, at about 10 mrad.

Among the heavier nuclei, most attention was given to lead. It was found that, once λ was chosen to give the correct value of σ_{abs}, as explained before, the height of the secondary maxima could be matched only when the real parts of the nuclear phase shifts inside the nucleus α_l were taken equal to zero. However, with $\alpha_l = 0$ the calculated minima are much deeper than the observed ones, as shown by the curve plotted in fig. 3. To be sure that the diffraction minima were not filled up as a result of multiple scattering in the target, a measurement was done with a target of only 0.3 mm. No modification of the diffraction pattern was found. The partial filling of the first diffraction minimum is due to the Coulomb contribution to the scattering amplitude (17). With $\alpha_l \neq 0$, and proportional to β_l, i.e. with a not negligible real part in the nuclear scattering amplitude, the minima can be filled up, but at the expense of making the calculated cross sections at the maxima substantially greater than the observed ones. The filling of the minima is most probably due to the contribution of events with associated nuclear excitation [9]), which in our measurements could not be separated from the true elastic events. A discussion of the inelastic scattering is not attempted here.

It is conceivable that, still with a purely elastic model, a better fitting could be achieved with a distribution of nuclear matter that at R does not drop suddenly to zero. However, the improvement could not be great, because as it can be seen from equation (19), even a uniform density distribution already gives rise to a transparent edge $\approx \lambda^2/8R$ thick ($\approx$ 0.1 fm for Pb).

Another cause of deformation of the scattering patterns is the non-sphericity of the nuclei. The difference between the pattern presented by $^{207.2}$Pb, a mixture of isotopes either magic-magic or nearly so, and that presented by $^{238.0}$U, whose numbers of protons and neutrons are far from the magic ones, is striking.

The incoherent scattering in heavy nuclei is relatively so small, in comparison with the coherent scattering, that it cannot be noticed even at the largest angles observed in the present experiment, except perhaps in the case of Cu, where $N(A)$ is found to be ≈ 6.7. The values of $N(A)$ quoted in parentheses in table 1 for Pb and U are those deduced from the empirical eq. (14) and do not appear to be in contradiction with the data of fig. 3.

6. Total Cross Sections

The strong interaction total cross sections of protons on nuclei were measured with the same beam and the same apparatus used for the measurement of the differential cross sections.

The transmission total cross section determined by the geometry of the trigger system (coincidences 1 2 3 4 5, see fig. 1) were obtained by replacing the scintillator C_4 by one without the hole and measuring the ratio of the counting rates 1 2 3 4 5 to 1 2 3, both with the targets in place and without them. The contribution to σ_{tot} measured in these condition was, e.g., for Al at 19.3 GeV/c, 0.517 b out of 0.687 b. The contributions for inelastic and elastic events included within the normal triggering counter system were obtained from the counting rates measured in the differential cross section runs.

To deduce the strong interaction total cross sections from these data, it is necessary to eliminate the contributions from electromagnetic interaction. For the light and medium elements, this was done by taking advantage of the separation between Coulomb and nuclear elastic scattering discussed in sect. 4. Of course, it was assumed that no contribution comes from a real nuclear scattering amplitude, i.e. that between Coulomb and nuclear scattering there is no interference. The total cross sections found after removal of this contribution are given in table 1, column 2.

The small angle contributions for the total cross sections of Cu and Pb (no transmission measurements were made with U) were obtained by assuming that at the smallest angles the nuclear differential cross section is that produced by a body of radius R, normalized to the optical theorem point (see eqs. (8) and (9)), the total cross section being obtained by iteration.

From the elastic differential cross sections, it was also possible to obtain the total elastic cross section σ_{el} and consequently the absorption cross section $\sigma_{\text{abs}} = \sigma_{\text{tot}} - \sigma_{\text{el}}$ (columns 3 and 4 of table 1). The elastic cross sections (nuclear coherent only) were evaluated by integrating over the solid angle the differential cross sections given by eqs. (8) and (9) for the light and medium nuclei and by eqs. (15)–(19) for the heavy nuclei, with the numerical values for the nuclear radii and the total cross sections given in table 1, but eliminating the Coulomb contributions. The numerical values of σ_{el} obtained in this way are given in table 1. They should be reliable within $\pm 5\%$.

It is gratifying to find that for Pb the elastic and the absorption cross sections are about equal, as expected for a nearly black body, and that the total cross section, when equated to $2\pi R^2$ gives $R = 7.3$ fm, in reasonable agreement with the value quoted in table 1.

The total and the elastic cross sections, as measured in the present experiment, are plotted in fig. 4 as functions of the mass number A. The absorption cross sections are also shown for completeness. On comparing with the $\propto A^{\frac{2}{3}}$ slope, it is evident that both σ_{tot} and σ_{abs} are about proportional to the areas covered by the nuclei. The steeper slope of σ_{el} shows that the nuclear transparency is rapidly decreasing with increasing A, the nuclei becoming opaque only for $A \approx 200$.

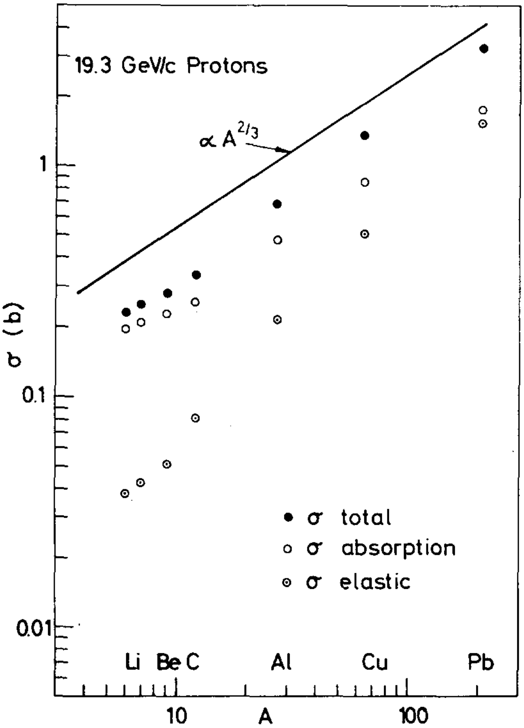

Fig. 4. The total, the elastic and the absorption cross sections measured in this experiment plotted as functions of the mass number A.

7. Conclusions

The validity of the optical model in interpreting the interaction of 20 GeV protons with nuclei is well proved by the results presented. However, the quantitative agreement between the predictions of the model and the experimental values is limited to the region within the first minimum, where slightly inelastic and quasi-elastic scattering are absent.

The values of the nuclear radii measured by proton scattering R_p can be compared with those measured [6]) by electron scattering R_e. For the lightest elements $R_p \approx R_e$, for the heaviest $R_p - R_e \approx 0.5$ fm. These radii do not fit very well a formula $R_p = r_0 A^{\frac{1}{3}}$.

It is also interesting to see that the differential cross sections at small angles are compatible with a real nuclear scattering amplitude equal to zero, though in the present case, this statement means only that at the smallest angles the contribution to the differential cross section of a real part of the nuclear scattering amplitude is not greater than 5–10% of the contribution of the imaginary part.

The existence of the quasi-elastic scattering cannot be described by an optical model. The knowledge of its dependence on the atomic number of the target can be put to use for the solution of practical problems. For instance, one might ask what is the advantage of using a target made with a light element in obtaining (i) monochromatic beams of scattered protons and (ii) secondaries not disturbed by further interactions within the nucleus in which they are produced.

In the first case, at angles with respect to the beam for which $|t| \gtrapprox 0.05\ (\mathrm{GeV}/c)^2$, the efficiency of a target is proportional to

$$\frac{(\mathrm{d}\sigma/\mathrm{d}\omega)_{\text{quasi elastic}}}{\sigma_{\text{abs}}} \propto \frac{A^{\frac{1}{3}}}{A^{\frac{2}{3}}} = \frac{1}{A^{\frac{1}{3}}}.$$

Thus, a Be target is about three times more efficient than a Pb target. In the second case, the probability that a secondary does not suffer an interaction in the same nucleus is proportional to the transparency, i.e. to $N(A)/A/\propto 1/A^{\frac{2}{3}}$, and the Be target is about nine times better than the Pb target.

Finally, the discussion of sect. 6 about total cross sections shows that reliable measurements of total and of absorption nuclear cross sections demand a detailed knowledge of the differential elastic cross sections.

The differences existing between the present values for the absorption cross sections of table 1 and those obtained earlier [10]) with a "bad geometry" absorption method, at 24 GeV, must be ascribed to a poor knowledge of the angular distributions of the elastic scattering. In fact the discrepancy between old and new data is greatest (up to 25% for Be) for the light elements, where the elastic scattering extends to larger angles, and becomes zero for Pb, where the elastic events are confined within angles so small that, in the previous experiment, they were never excluded by the counters defining the scattered beam.

We are indebted to P. Zanella for the development of the programmes, to A. E. Taylor for help and useful conversations in the early stage of the experiment and to P. Preiswerk for constant encouragement. We wish to thank the members of the Proton Synchotron division for their collaboration, J. Geibel for the beam design; F. Iselin, E. Långh, A. Maurer, P. Ponting and E. Schuller for producing the data registration system; R. Bell for programming help; C. A. Ståhlbrandt, J. L. Goodchild and M. Ferrat for the development of spark chamber circuitry, and R. Donnet for his work on the spark chambers and associated equipment. We are very grateful to T. E. Ericson for many discussions on the interpretation of the data.

References

1) W. M. Preston, R. Wilson and J. C. Street, Phys. Rev. **118** (1959) 579
2) G. Bellettini, G. Cocconi, A. N. Diddens, E. Lillethun, J. Pahl, J. P. Scanlon, J. Walters, A. M. Wetherell and P. Zanella, Phys. Lett. **14** (1965) 164
3) A. N. Diddens, IEEE Trans. on Nuclear Science NS12 No. 4 (1965) 170
4) F. Iselin, E. Langh, A. Maurer, P. Ponting and E. Schuller, Proc. Informal Meeting on Filmless Spark Chambers, CERN 64d30 (1964), p. 211
5) H. A. Bethe and J. Ashkin, in Experimental nuclear physics, vol. 1 ed. by E. Segre (Wiley, New York, 1952) p.p. 166, 290
6) R. Herman and R. Hofstadter, High-energy electron scattering tables, (Stanford University Press, 1960, p. 62
7) E. Clementel and A. Coen, Nuovo Cim. **10** (1953) 988
8) H. Bethe, Ann. of Phys. **3** (1958) 190
9) T. H. Schucan, Nuclear Physics **61** (1965) 417;
I. Zh. Petkov, Dubna Report P–2037 (1965)
10) A. Ashmore, G. Cocconi, A. N. Diddens and A. M. Wetherell, Phys. Lett. **5** (1960) 576